NUCLEAR STRUCTURE – "AB INITIO"

H. FELDMEIER AND T. NEFF
Gesellschaft für Schwerionenforschung mbH
Planckstr. 1, D-64291 Darmstadt, Germany
E-mail: h.feldmeier@gsi.de, t.neff@gsi.de

R. ROTH
Institut für Kernphysik
Schlossgartenstr. 9, D-64289 Darmstadt, Germany
E-mail: robert.roth@physik.tu-darmstadt.de

An ab-initio description of atomic nuclei that solves the nuclear many-body problem for realistic nuclear forces is expected to possess a high degree of predictive power. In this contribution we treat the main obstacle, namely the short-ranged repulsive and tensor correlations induced by the realistic nucleon-nucleon interaction, by means of a unitary correlation operator. This correlator applied to uncorrelated many-body states imprints short-ranged correlations that cannot be described by product states. When applied to an observable it induces the correlations into the operator, creating for example a correlated Hamiltonian suited for Slater determinants. Adding to the correlated realistic interaction a correction for three-body effects, consisting of a momentum-dependent central and spin-orbit two-body potential we obtain an effective interaction that is successfully used for all nuclei up to mass 60. Various results are shown.

1. Introduction

In the last years exact *ab initio* calculations of light nuclei have become feasible with Greens Function Monte Carlo calculations[1] and in the No-Core Shell Model [2]. Here realistic interactions that fit the nucleon-nucleon scattering data and the deuteron properties are used [3,4]. Additional three-body forces are needed and are adjusted to the spectra of nuclei. Chiral perturbation promises to provide a consistent derivation of two- and three-body forces [5,6].

2. The Unitary Correlation Operator Method (UCOM)

Our aim is to perform *ab initio* calculations of larger nuclei with realistic interactions like the Bonn or Argonne potentials in a Hartree-Fock picture or a many-body approach with configuration mixing.

The repulsive core and the strong tensor force of the nuclear interaction induce strong short-range radial and tensor correlations in the nuclear many-body system. These correlations are in the relative coordinates $\boldsymbol{r}_{ij} = \boldsymbol{r}_i - \boldsymbol{r}_j$ and thus can not be represented by products of single-particle states like Slater determinants

$$\big|\,\Psi\,\big\rangle = \mathcal{A}\left\{\big|\,q_1\,\big\rangle \otimes \ldots \otimes \big|\,q_A\,\big\rangle\right\} \tag{1}$$

that are usually used as many-body states in Hartree-Fock or a shell-model calculations. $\mathcal{A}$ denotes the antisymmetrization operator and $\big|\,q_i\,\big\rangle$ the single-particle states.

Instead we treat the radial and tensor correlations explicitly by a unitary correlation operator C that acts on uncorrelated product states $\big|\,\Psi\,\big\rangle$

$$\big|\,\hat{\Psi}\,\big\rangle = C\,\big|\,\Psi\,\big\rangle \tag{2}$$

such that the many-body state $\big|\,\hat{\Psi}\,\big\rangle$ contains the short ranged correlations. For the correlator we make the following ansatz

$$C = C_\Omega \cdot C_r = \exp\Big\{-\mathrm{i}\sum_{i<j} g_{\Omega\,ij}\Big\} \cdot \exp\Big\{-\mathrm{i}\sum_{i<j} g_{r\,ij}\Big\}\ . \tag{3}$$

It is the product of a radial correlator C_r and a tensor correlator C_Ω, both, expressed with a hermitian two-body generator in the exponent.

2.1. *Cluster expansion*

As the ansatz for the correlator contains a two-body operator in the exponent any correlated operator will contain many-body parts. For example a Hamiltonian consisting of one- and two-body parts will turn into

$$\begin{aligned}\hat{H} &= C^\dagger H C = C^\dagger\Big(\sum_i T_i + \sum_{i<j} V_{ij}\Big)C \qquad (4)\\ &= \sum_i T_i + \sum_{i<j}\hat{T}^{[2]}_{ij} + \sum_{i<j<k}\hat{T}^{[3]}_{ijk} + \cdots + \sum_{i<j}\hat{V}^{[2]}_{ij} + \sum_{i<j<k}\hat{V}^{[3]}_{ijk} + \cdots\ ,\end{aligned}$$

where the upper script $^{[n]}$ indicates irreducible n-body operators. Here we introduce an approximation by keeping terms only up to two-body operators. This approximation should be good for systems where the range of

the correlator ($g_{r\,ij} = 0$ and $g_{\Omega\,ij} = 0$ for $r_{ij} > R_c$) is short compared to the mean particle distances. In that case the probability to find 3 particles simultaneously within the correlation range R_c is small.

2.2. *Radial correlator*

The radial correlator C_r (described in detail in [7]) shifts a pair of particles in the radial direction away from each other so that they get out of the range of the repulsive core. To perform the radial shifts the generator of the radial correlator uses the radial momentum operator p_r together with a shift function $s(r)$ that depends on the distance of the two nucleons.

$$g_{r\,ij} = \frac{1}{2}\Big(p_{r\,ij}s(r_{ij}) + s(r_{ij})p_{r\,ij}\Big) \tag{5}$$

The shift function $s(r)$ is optimized to the potential under consideration. It is large for short distances and will vanish at large distances.

The effect of the transformation $\big|\,\Psi\,\big\rangle \rightarrow C_r\big|\,\Psi\,\big\rangle$ is shown in the upper part of Fig. 1 where the two-body density $\rho^{(2)}_{S,T}$ is displayed as a function of the distance vector ($\boldsymbol{r}_1$–$\boldsymbol{r}_2$) between two nucleons in ^{4}He. On the l.h.s. $\rho^{(2)}_{S,T}$ is calculated with the shell-model state $\big|\,(1s_{1/2})^4\,\big\rangle$ that is just a product of 4 Gaussians. It has a maximum at zero distance which is in contradiction to the short ranged repulsion of the interaction. This inconsistency is removed by application of the radial correlator C_r that moves density out of the region where the potential is repulsive. The corresponding kinetic, potential and total energies are displayed in the lower part of the figure for three nuclei. The radially correlated kinetic energy $\big\langle\, C_r^\dagger T C_r\,\big\rangle$ increases somewhat compared to $\big\langle\, T\,\big\rangle$ but this is overcompensated by the gain of about -25 MeV per particle in the correlated potential energy. Nevertheless the nuclei are still unbound.

2.3. *Tensor correlator*

The tensor force in the $S=1$ channels of the nuclear interaction depends on the spins and the spatial orientation $\hat{\boldsymbol{r}} = (\boldsymbol{r}_1–\boldsymbol{r}_2)/(|\boldsymbol{r}_1–\boldsymbol{r}_2|)$ of the nucleons via the tensor operator

$$S_{12}(\hat{\boldsymbol{r}},\hat{\boldsymbol{r}}) = 3(\boldsymbol{\sigma}_1\cdot\hat{\boldsymbol{r}})(\boldsymbol{\sigma}_2\cdot\hat{\boldsymbol{r}}) - (\boldsymbol{\sigma}_1\cdot\boldsymbol{\sigma}_2) = 2\,\Big(3(\boldsymbol{S}\cdot\hat{\boldsymbol{r}})^2 - \boldsymbol{S}^2\Big)\,. \tag{6}$$

An alignment of $\hat{\boldsymbol{r}}$ with the direction of the total spin $\boldsymbol{S} = \frac{1}{2}(\boldsymbol{\sigma}_1+\boldsymbol{\sigma}_2)$ is favored energetically. The tensor correlator $C_\Omega = \exp\Big\{-\mathrm{i}\sum_{i<j} g_{\Omega\,ij}\Big\}$,

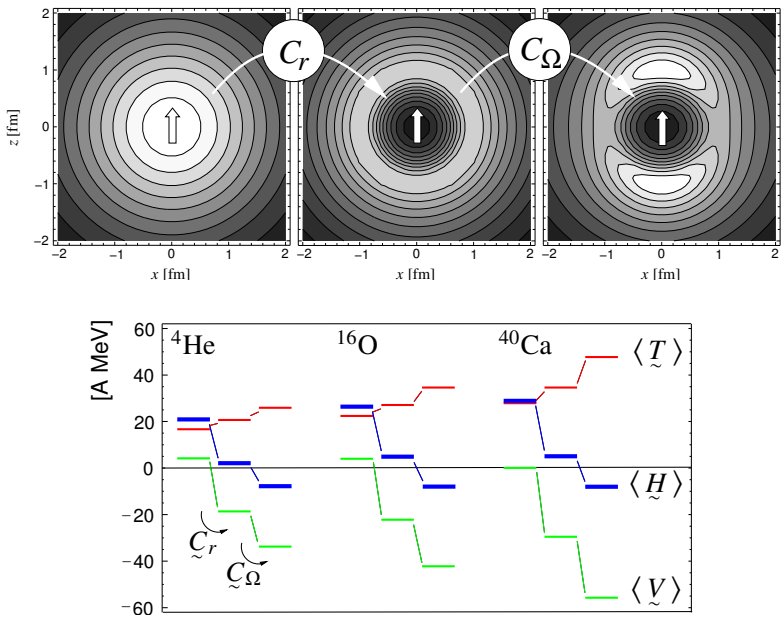

Figure 1. Upper part: Two-body density $\rho^{(2)}_{S,T}(\boldsymbol{r}_1-\boldsymbol{r}_2)$ of ^{4}He for a pair of nucleons with isospin $T=0$ and parallel spins, $S=M_S=1$. Bright ares denote large probabilities. Arrow indicates spin direction and $(x,y,z) = (\boldsymbol{r}_1-\boldsymbol{r}_2)$ relative distance vector. Lower part: corresponding kinetic, potential and total energies per particle of ^{4}He, ^{16}O and ^{40}Ca, without, with radial, and with radial and tensor correlations (Bonn-A potential).

defined by the generator

$$g_{\Omega\,ij} = \vartheta(r_{ij})\frac{3}{2}\Big((\boldsymbol{\sigma}_i\boldsymbol{p}_{\Omega\,ij})(\boldsymbol{\sigma}_j\boldsymbol{r}_{ij}) + (\boldsymbol{\sigma}_i\boldsymbol{r}_{ij})(\boldsymbol{\sigma}_j\boldsymbol{p}_{\Omega\,ij})\Big)\ , \qquad (7)$$

achieves this alignment by shifts perpendicular to the relative orientation $\hat{\boldsymbol{r}}_{ij}$. For that the generator of the tensor correlator uses a tensor operator constructed with the orbital part of the relative momentum operator $\boldsymbol{p}_{\Omega\,ij} = \boldsymbol{p}_{ij}-\boldsymbol{p}_{r\,ij}$. The r-dependent strength and the range of the tensor correlations is controlled by $\vartheta(r)$. For details see [8].

The application of the tensor correlator C_Ω leads to the two-body density depicted in the right hand contour plot of Fig. 1. One may visualize the action of C_Ω as a displacement of probability density from the 'equator' to both 'poles', where the spin of the $S=1$ component of the nucleon pair defines the 'south-north' direction. Again this costs kinetic energy but now the many-body state is in accord with the tensor interaction and one gains the binding needed to end up with about -8 MeV per particle.

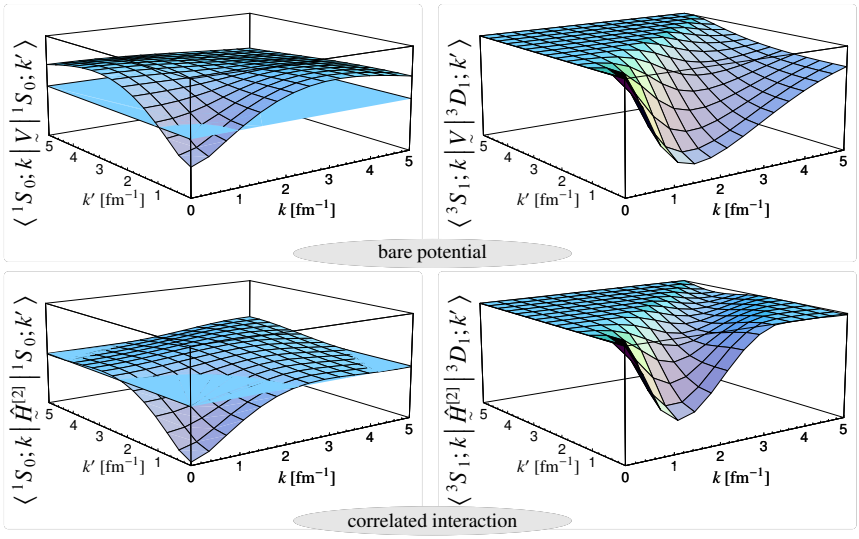

Figure 2. Bare and correlated Argonne V8' interaction in momentum-space. Matrix elements range from -2 to +2 fm^{-1} on the l.h.s. and from -1.5 to 0 fm^{-1} on the r.h.s.

3. Interaction in momentum-space

The inclusion of the short-range correlations achieves a *pre-diagonalization* of the nuclear hamiltonian that is illustrated in Fig. 2. On the l.h.s. the effect of the radial correlations is shown in the $^1S_0$ channel. The correlated interaction evaluated in momentum-space is more attractive and does not possess the large off-diagonal matrix elements of the bare interaction. Also the tensor components of the correlated Hamiltonian do not connect to high momenta as is illustrated with the matrix elements between the $^3S_1$ and the $^3D_1$ channel. The correlated interaction is therefore a low-momentum interaction very similar to the V_{low-k} [9].

4. Effective interaction

To test the two-body approximation we performed no-core shell model calculations with the correlated AV8' interaction for ^{4}He and compared with exact results [10,11]. It turned out that neglecting the $n = 3$- and 4-body parts $\hat{T}^{[n]}$ and $\hat{V}^{[n]}$ of the correlated Hamiltonian leads to an overbinding which is of the same order as the contribution from genuine 3-body forces. Because of the low-momentum nature of the correlated Hamiltonian $\hat{H}^{C2} = T + \hat{T}^{[2]} + \hat{V}^{[2]}$ it can be used directly with simple model spaces

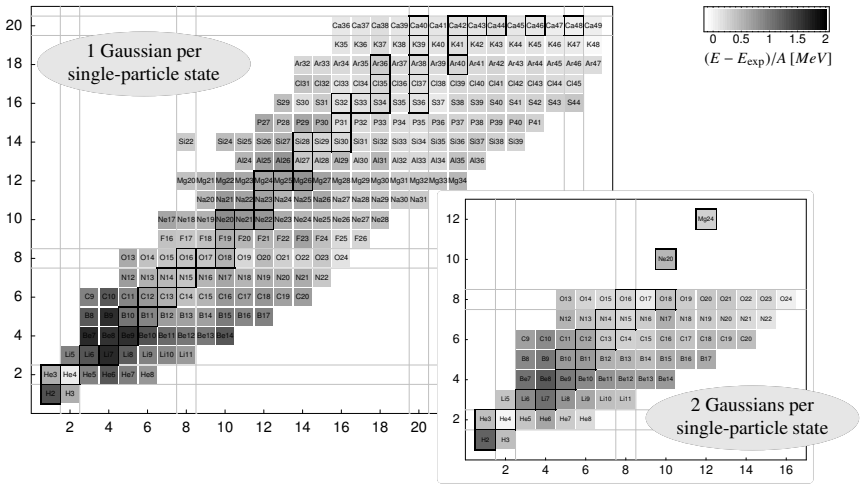

Figure 3. Deviation of mean-field binding energies from measured ones.

built of Slater determinants. The effects of missing higher-order contributions to the correlated interaction and of genuine three-body forces is for now effectively described by a momentum-dependent central and spin-orbit correction H_{corr} with four parameters adjusted to four doubly magic nuclei. The resulting effective interaction $\hat{H}_{eff} = \hat{H}^{C2} + H_{corr}$ is used for all nuclei up to mass number 60. The expectation value of H_{corr} is typically 15% of the correlated interaction energy.

5. Hartree-Fock calculations

For the nuclei listed in the nuclear chart Fig. 3 we minimized the expectation value $\langle\, \Psi \,|\, \hat{H}_{eff} - T_{cm} \,|\, \Psi \,\rangle / \langle\, \Psi \,|\, \Psi \,\rangle$ with respect to all parameters of the single-particle states

$$\langle\, \boldsymbol{x} \,|\, q \,\rangle = \sum_i c_i \exp\left\{ -\frac{(\boldsymbol{x} - \boldsymbol{b}_i)^2}{2a_i} \right\} |\, \chi_i \,\rangle \otimes |\, \xi \,\rangle \tag{8}$$

that are contained in the Fermionic Molecular Dynamics [12] state $|\, \Psi \,\rangle$ (Eq. (1)). The summation is either for one or for two independent Gaussians per single-particle state.

The inclusion of a second Gaussian improves the masses of p-shell nuclei substantially (inset of Fig. 3). The largest deviations occur for nuclei with an α-cluster structure like ^{8}Be or ^{12}C or for intrinsically deformed nuclei at

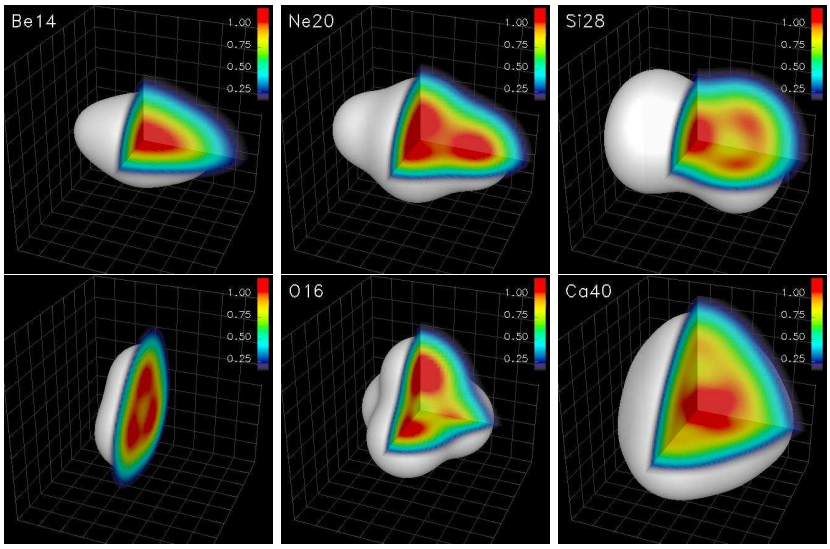

Figure 4. One-body densities of intrinsic states. Upper part: PAV calculation ^{14}Be, ^{20}Ne, ^{28}Si (local minimum); lower part: VAP calculation ^{12}C, ^{16}O, ^{40}Ca.

the middle of the *sd*-shell. Some examples of intrinsic shapes are displayed in the upper half of Fig. 4. In ^{14}Be the extra six neutrons have pulled together the well localized pair of α's that form ^{8}Be. The peanut like shape for ^{28}Si is a local minimum.

6. Projection after variation and variation after projection

To improve the many-body Hilbert space we project on spin and parity after variation (PAV). We also perform variation after projection (VAP) calculations in the sense of the generator coordinate method. The intrinsic state is minimized here with constraints on radius, dipole moment, quadrupole or octupole moment.

With the above described effective interaction ^{16}O gains in a VAP calculation about 5 MeV in binding by forming α-clusters (see lower part of Fig. 4) compared to the spherical closed-shell configuration which represents the energy minimum in the PAV case. Even for ^{40}Ca VAP leads to a deformation towards a tetrahedron of ten α's which however are much more amalgamated than in ^{16}O (Fig. 4).

In a next step the different intrinsic shapes obtained in the VAP process can be used to perform multiconfiguration calculations.

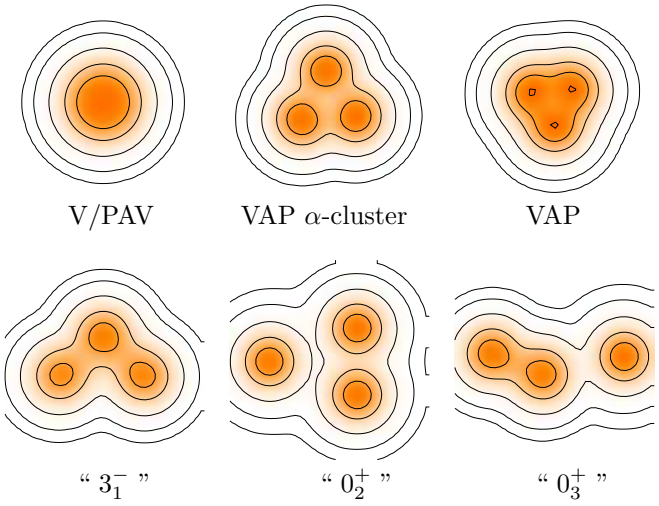

Figure 5. One-body densities of intrinsic ^{12}C states.

A very interesting nucleus is ^{12}C for which the shell-model configuration $(1s_{1/2})^4(1p_{3/2})^8$ is competing with the 3-α cluster structure [13,14]. Like in ^{16}O the PAV ground state of ^{12}C turns out to be a spherical shell-model state (Fig. 5, V/PAV). However, variation after projection leads to a triangular shape made of three α's (Fig. 5, VAP) and 7.2 MeV of additional binding as indicated in Table 1. A pure α-cluster configuration obtained in a VAP calculation has larger distances between the α-clusters and is 4.3 MeV less bound than the shell-model configuration. The difference to the full VAP is due to the polarization of the α-clusters. The description of this polarization is significantly improved by using two Gaussians per single-particle state.

The description of the excited states requires an enlarged Hilbert space. Multiconfiguration calculations with the configurations shown in the lower part of Fig. 5 show only a small increase in binding for the groundstate

	E_b [MeV]	r_{charge} [fm]	$B(E2)$ [e^2fm^4]
V/PAV	84.7	2.33	-
VAP α-cluster	80.4	2.66	56.3
VAP	91.9	2.38	24.7
Multiconfig	93.4	2.50	40.0
Exp	92.2	2.47	39.7 ± 3.3

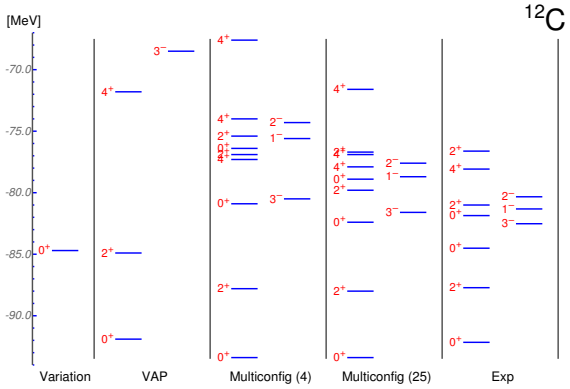

Figure 6. Calculated and experimental level scheme for ^{12}C.

but have a significant effect on the radius and the $B(E2)$ value for the $0_1^+ \longrightarrow 2_1^+$ transition. The additional configurations have been chosen to give lowest energies for the 3_1^- and the second and third 0^+ states. We find 3 α-cluster structures for the 0_2^+ state and ^{8}Be + α-cluster structures for the 0_3^+ state. For an improved description of these states a larger number of configurations with greater distances between the α's is needed. This is consistent with an assumed Bose condensed state[15] for the 0_2^+ state.

References

1. S.C. Pieper, R.B. Wiringa, *Ann. Rev. Nucl. Part. Sci.* **51**, 53 (2001).
2. P. Navratil, W.E. Ormand, *Phys. Rev.* **C68** 034305 (2003).
3. R. Machleidt, *Phys. Rev.* **C63** 024001 (2001).
4. R. Wiringa, V. Stoks, R. Schiavilla, *Phys. Rev* **C51** 53, 2001.
5. D.R. Entem, R. Machleidt, *Phys. Rev.* **C68** 041001 (2003).
6. W. Glöckle et al., *in these proceedings*
7. H. Feldmeier, T. Neff, R. Roth, J. Schnack, *Nuc. Phys.* **A632**, 61 (1998).
8. T. Neff, H. Feldmeier, *Nuc. Phys.* **A713**, 311 (2003).
9. S.K. Bogner, T.T.S. Kuo and A. Schwenk, *Phys. Rept.* **386**, 1 (2003).
10. T. Neff, H. Feldmeier, *Proc. of the International Workshop XXXI on Nuclear Structure and Dynamics at the Limits, Hirschegg, Austria, January 12-18, 2003*
11. H. Kamada et al., *Phys.Rev.* **C64** 044001 (2001).
12. H. Feldmeier and J. Schnack, *Rev. Mod. Phys.* **72**, 655 (2000).
13. Y. Kanada-En'yo, *Phys. Rev. Lett.* **81** 5291 (1998).
14. N. Itagaki et al., *Nuc. Phys.* **A719**, 205c (2003).
15. Y. Funaki, A. Tohsaki, H. Horiuchi, P. Schuck, G. Röpke, *Phys. Rev.* **C67** 051306 (2003).